Iran Polym J (2016) 25:157–167
DOI 10.1007/s13726-015-0410-8

ORIGINAL PAPER

Compatibilization effectiveness of maleated polypropylene compared to organoclay in PBT/PP blends

Armin Hajibaba[1] · **Mahmood Masoomi**[1] · **Hossein Nazockdast**[2]

Received: 13 July 2015 / Accepted: 19 December 2015 / Published online: 25 January 2016

Abstract The compatibilization efficiency of a conventional compatibilizer (PP-grafted maleic anhydride) is compared with an organoclay of hydrophilic modifier (Cloisite 30B) in poly(butylene terephthalate)/polypropylene (PBT/PP) immiscible polymer blend. Moreover, the effect of PP-grafted maleic anhydride (PP-*g*-MA) on localization of Cloisite 30B organoclays is investigated, in this research. Accordingly, PBT/PP blends containing PP-*g*-MA, organoclay and PP-*g*-MA/organoclay are prepared by melt mixing method. According to morphological analysis, organoclays are more efficient than PP-*g*-MA in dispersion and distribution of droplets in PBT/PP blend. Additionally, the size of dispersed-droplets in PBT/PP/organoclay nanocomposite is lower than PBT/PP/PP-*g*-MA/organoclay sample. From X-ray diffractometry (XRD) and transmission electron microscopy illustrations, it is shown that organoclays represent the higher level of intercalation structure in PBT/PP/organoclay compared to PBT/PP/PP-*g*-MA/organoclay nanocomposite. PBT/PP/Organoclay nanocomposite indicates higher viscosity and elasticity in comparison with PBT/PP/PP-*g*-MA/organoclay, as well. The present subject can be explained by the role of PP-*g*-MA in transferring some parts of organoclays from PBT matrix into PP droplets which hinders the break-up of dispersed-droplets. According to non-linear viscoelastic properties, PBT/PP/organoclay sample shows stronger stress overshoots than PBT/PP/PP-*g*-MA/organoclay in start-up of shear flow. Modified De Kee-Turcotte model is studied to investigate the yield stress and viscoelastic behavior of different samples. PBT/PP/Organoclay nanocomposite shows higher yield stress compared to PBT/PP blend filled by PP-*g*-MA/organoclay system.

Keywords Compatibilization · Cloisite 30B · PP-*g*-MA · PBT/PP blend · Morphology

Introduction

Polymer blending is a useful method to produce new polymeric materials with specific properties [1]. Blending of polyolefin with poly(alkyl terephthalate) is a technique to improve mechanical properties of poly(ethylene terephthalate) (PET), poly(butylene terephthalate) (PBT) and poly(trimethylene terephthalate) (PTT) [2–4]. Among this, PBT/PP blend, like the most polymeric pairs, is considered to be immiscible [5, 6]. As a result, the compatibilization of PP and PBT is a very crucial route to achieve ultimate desired properties.

Block or graft copolymers utilization is a traditional route to attain compatibility between polymeric materials [7, 8]. Compatibilizers help to form finer morphology by anchoring along the interface and coalescence hindrance of droplets, in immiscible polymer blends. Sun et al. [9] examined the compatibilization efficiency of various compatibilizers containing acrylic acid (AA), glycidyl methacrylate (GMA) and maleic anhydride (MA) in PBT/PP polymer blends. According to their research, PP-*g*-GMA is considered to be the most effective compatibilizer. Papadopoulou et al. [10] compared the compatibilization efficiency of SEBS-*g*-MA, PP-*g*-MA and LLDPE-*g*-MA in PET/PP blend. They showed that SEBS-*g*-MA performance

✉ Mahmood Masoomi
mmasoomi@cc.iut.ac.ir

[1] Chemical Engineering Department (Polymer Group), Isfahan University of Technology, Isfahan 84156-83111, Iran

[2] Polymer Engineering Department, Amirkabir University of Technology, P.O. Box: 15875-4413, Tehran, Iran

is the best amongst the other compatibilizers. In addition to block or graft compatibilizers, inorganic solid particles can play the compatibilization role in polymer blends [11–13]. Some researchers [14–16] reported the effect of organoclays on compatibilization and properties of the polymer blends. Hong et al. [13] showed the role of organoclays in break-up and coalescence suppression of droplets in PBT/PE blends. Based on their research, the localization of organoclays at the interface ends up with formation of the interfacial phase. The heterogeneous distribution of clays along the interface can reduce the interfacial tension. Moreover, the solid entity of organoclays along with their high aspect ratio can hinder the coalescence of droplets which reflects on their reduced droplet size. Based on the results of Xue et al. [4], organically modified clays are mainly located at the interface of PTT/PP blend and PTT matrix. They showed that when PP is the dispersed-phase, the size of PP droplets will be decreased with increasing of organoclay concentration. Additionally, by inclusion of 5 wt% of PP-*g*-MA there would be finer morphology of PTT/PP/organoclay nanocomposites developed and more exfoliation of organoclays at the interface. Calcagno et al. [16] declared that clay is dominantly located at the interface of PP/PET blends and in the PET phase. The incorporation of PP-*g*-MA as compatibilizer improved the dispersion of clay in PP/PET compared to uncompatibilized nanocomposite. The nanocomposite containing compatibilizer leads to interconnected morphology, as well. The remarkable properties of intercalated/exfoliated organoclays together with compatibilization effect make them as ideal fillers for polymeric systems [17–19].

The influence of compatibilizers and nanoparticles on morphology and rheological behavior of immiscible polymer blends has been published, numerously. But nobody has discussed and compared the compatibilization effectiveness of conventional compatibilizers with those of solid nanoparticles, yet. In addition, there are scrimpy researches regarding the effect of compatibilizers on dispersion and localization of organoclays in polymer blends. Due to the importance of compatibilization in both academic and industrial fields, we explore the compatibilization efficiency of PP-*g*-MA (a conventional compatibilizer), Cloisite 30B (organoclay) and PP-*g*-MA/organoclay in PBT/PP blends. Moreover, the role of PP-*g*-MA in dispersion and localization of Cloisite 30B layers is investigated in this research.

Experimental

Materials

Poly(butylene terephthalate) used as matrix was supplied by Eurotec® under the grade of PB-NL70. Its density was 1.33 g cm^{-3} with the melting point at 225 °C. Isotactic polypropylene with the grade of V30S, as dispersed-phase, was obtained from Marun Petrochemical Company. The density of PP was 0.9 g cm^{-3} with its MFI of 16 g/10 min and HDT at 95 °C. Organoclay with hydrophilic modifier (Cloisite 30B) was provided by Southern Clay Company of USA. Cloisite 30B was modified with methyl tallow bis-2-hydroxyethyl, quaternary ammonium with an amount of 90 meq/100 g. Maleated polypropylene (CM-1120H, M_w: 124,200 g mol^{-1}, MFI: 80 g/10 min, MAH graft ratio 0.5–1.0 wt%) used as compatibilizer was obtained from the Honam Petrochemical of Korea. Irganox 1010 used as anti-oxidant, was obtained from Ciba of Singapore.

Sample preparation

The samples were prepared by melt blending method in a Brabender internal mixer at 245 °C and rotor speed of 60 rpm. The composition of samples is listed in Table 1. All composite ingredients were dried in a vacuum oven for 24 h at 80 °C. First, PBT and PP were dry mixed and charged to the chamber. Melt blending lasted around 6 min. After the blending of PBT and PP, the other ingredients (organoclay, compatibilizer and organoclay/compatibilizer) were introduced into the mixer and melt compounding process was carried out for 9 min. Moreover, 0.2 wt% of Irganox 1010, as anti-oxidant, was used to prevent degradation. For PBT/Cloisite 30B and PP/Cloisite 30B nanocomposites, polymeric component and nanoparticles were charged into the mixer, simultaneously and melt mixing was done for 10 min (at the same temperature and rotor speed). At last, the blends were hot pressed at 245 °C for 10 min into a mold with the thickness of 1 mm and then annealed to room temperature.

Characterization methods

Wide angle X-ray diffraction (WAXD) experiments were performed by Phillips X′Pert MPD. The diffractometer was equipped by Cobalt tube with the wavelength of 1.78 Å, voltage of 40 kV and current of 40 mA. The diffractometer

Table 1 Composition of samples used in the present research

Sample	PBT (wt%)	PP (wt%)	Cloisite 30B (wt%)	PP-*g*-MA (wt%)
B30B5	100	0	5	0
P30B5	0	100	5	0
BP	80	20	0	0
BPC5	80	15	0	5
BP30B5	80	20	5	0
BP30B5C5	80	15	5	5

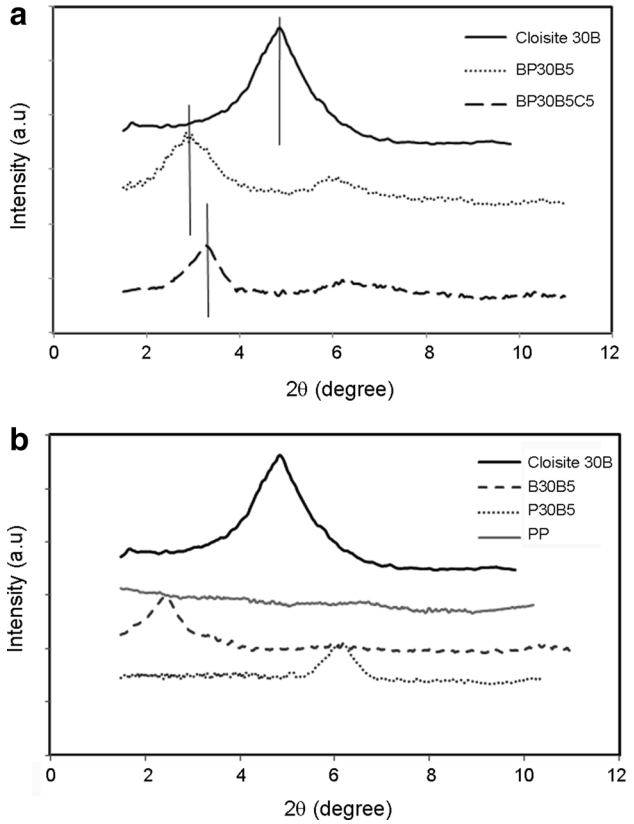

Fig. 1 XRD patterns of **a** neat Cloisite 30B, PBT/PP/Cloisite 30B, PBT/PP/PP-*g*-MA/Cloisite 30B and **b** PBT/Cloisite 30B, PP/Cloisite 30B and PP

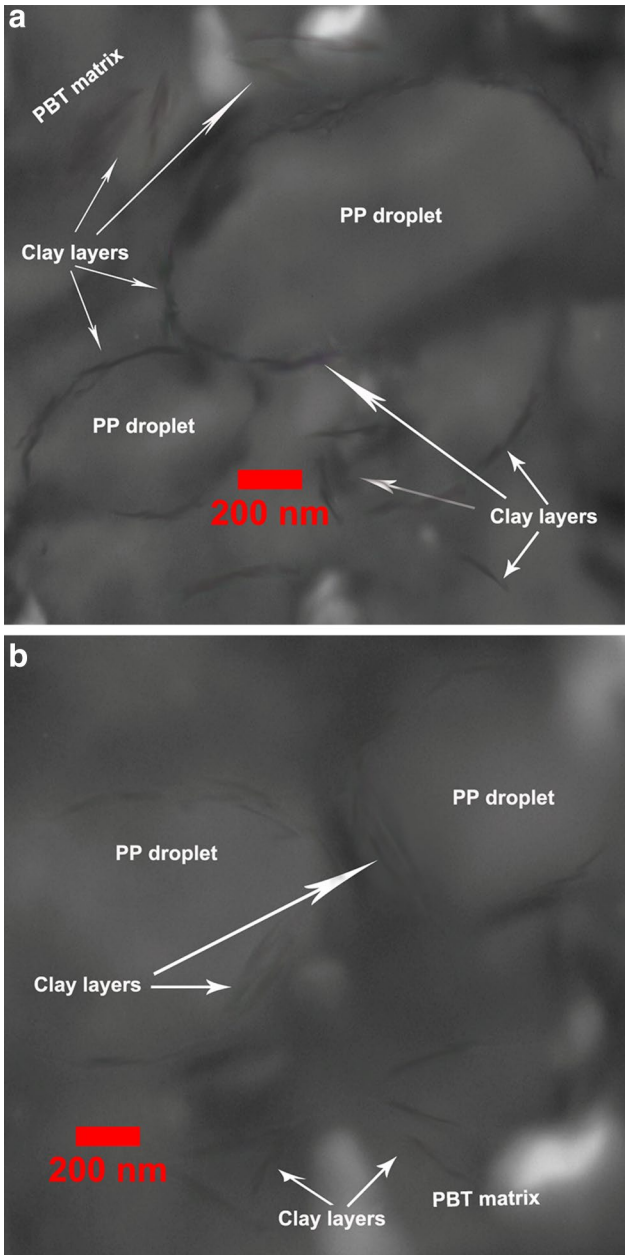

Fig. 2 TEM photographs of **a** BP30B5 and **b** BP30B5C5 nanocomposites

was scanned in the 2θ range from 1.5° to 10°, at the rate of 1° min^{-1}, at ambient temperature and measurements were recorded every 0.02°.

The morphology of samples was studied using a Vega/Tescan scanning electron microscope (SEM) of USA. The samples were cryogenically fractured after a storage time in liquid nitrogen of 15 min. The fracture surfaces were coated with gold for enhanced conductivity using a sputter coater.

Transmission electron microscope, Zeiss TEM operated at 80 kV, was used to investigate the dispersion state of nanoclays. TEM specimens were prepared by cryogenically microtomed at −70 °C.

The linear melt rheology of samples was studied by RMS, Paar Physica US200. All measurements were performed at 245 °C in parallel plate fixture with diameter equal to 25 mm and 1 mm gap. The linear viscoelastic region was conducted by plotting storage modulus in a strain amplitude sweep test. The non-linear rheological properties of nanocomposites were evaluated by start-up of flow and stress relaxation experiments. In start-up of flow, the nanocomposites were applied at constant shear rate and shear flow was monitored by the time. In the stress relaxation test, the nanocomposites were held at a constant strain (5 %) and relaxation modulus was plotted as a function of time.

Fourier transform infrared spectroscopy (FTIR) was carried out in a FTIR Bruker spectrophotometer (model Equinox 55) in the range of 650–4000 cm^{-1}. The specimens for this test were prepared by ATR technique.

Results and discussion

X-ray measurements

X-ray diffractometry was used to investigate the state of Cloisite 30B layers in nanocomposites. Figure 1a shows the XRD curves of pristine Cloisite 30B, PBT/PP/Cloisite 30B and PBT/PP/PP-*g*-MA/Cloisite 30B. The diffraction peak of the (001) reflections of Cloisite 30B is evident at 4.85° attributed to d_{001} spacing of 21.19 Å, calculated based on Bragg's formula. Obviously, the characteristic peak of Cloisite 30B has been decreased to 2.88° (*d*-spacing of 35.6 Å) and 3.27° (*d*-spacing of 31.22 Å) for BP30B5 and BP30B5C5 nanocomposites, respectively. The second peak observed at $5.5° < 2\theta < 7°$ may be attributed to the thermal degradation of Cloisite 30B modifying alkyl ammonium groups at 245 °C (processing temperature). The increment of *d*-spacing is observed for both types of nanocomposites. It seems that good affinity between hydroxyl and carboxyl end groups of PBT, and hydroxyl ethyl groups of Cloisite 30B (CH_2CH_2OH) is responsible for the intercalation of PBT chains into the gallery of Cloisite 30B layers. Comparing the XRD patterns of BP30B5 and BP30B5C5 indicates that adding PP-*g*-MA reduces the level of intercalation structure in BP30B5C5 nanocomposite. One may conclude that the presence of PP-*g*-MA as compatibilizer transfers some parts of organoclays from PBT matrix to PP phase where ability in Cloisite 30B intercalation is lower. The similar behavior was reported by Nazockdast et al. [20] for polylactide/polyethylene/organoclay nanocomposites

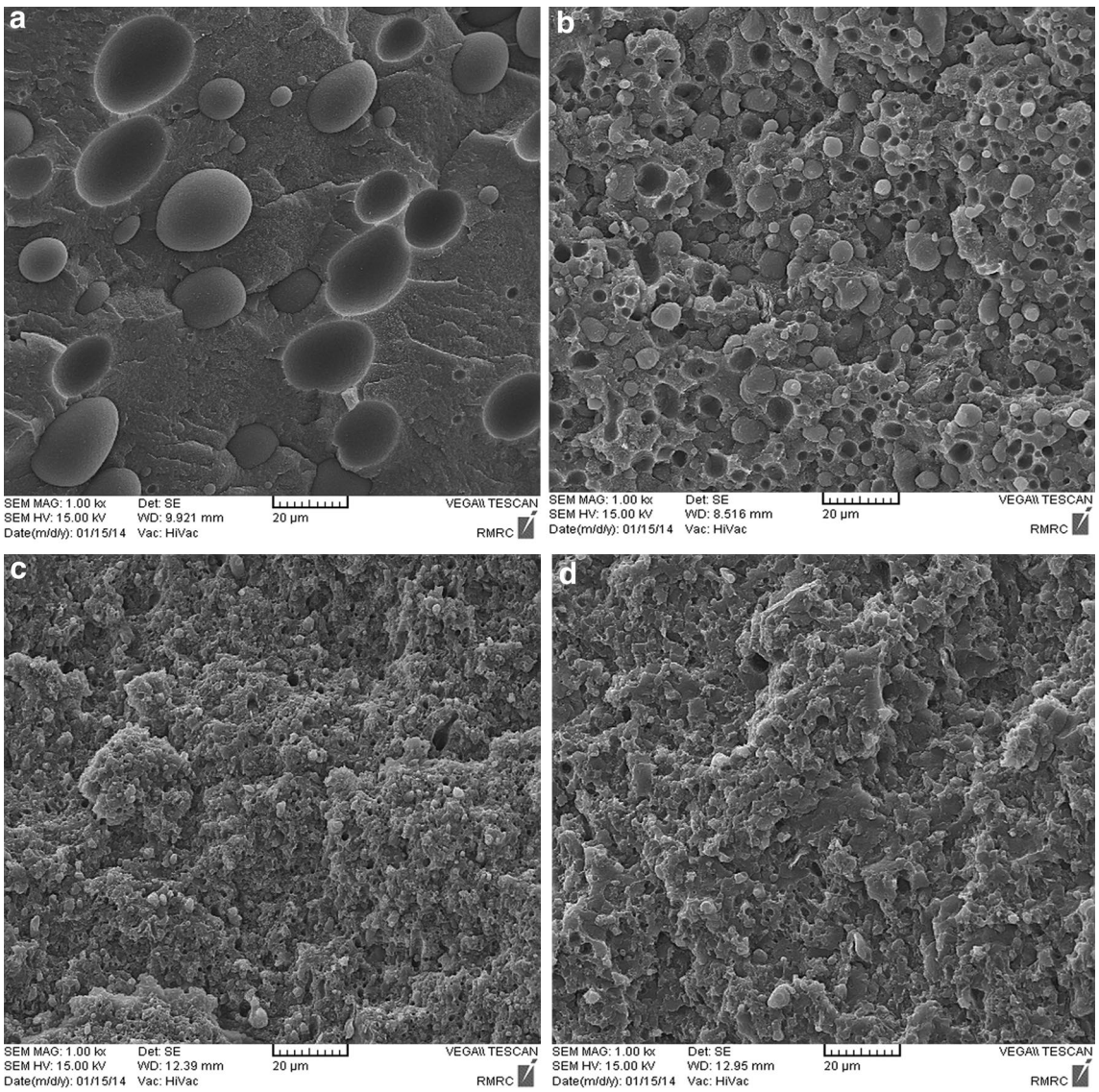

Fig. 3 SEM micrographs of **a** BP, **b** BPC5, **c** BP30B5 and **d** BP30B5C5

compatibilized by maleated polyethylene (PE-*g*-MA). On the other hand, Xue et al. [4] declared the finer morphology of PTT/PP/Cloisite 25A nanocomposite with higher exfoliation structure in the presence of 5 wt% PP-*g*-MA. They suggested that using 5 wt% PP-*g*-MA in PTT/PP/Cloisite 25A nanocomposite results in forming phase border-lines in polygonal shape at the interface. Therefore, more investigations would be needed to evaluate the effect of compatibilizers on morphology and viscoelastic behavior of polymer blend nanocomposites.

The X-ray diffraction of PBT and PP filled by 5 wt% of Cloisite 30B is illustrated in Fig. 1b. As it is clear, the characteristic peak of organoclay in PBT/organoclay sample shifts to lower angles (2.43°) which means great capability of PBT chains in improvement of Cloisite 30B intercalation. On the other hand, the main peak location of Cloisite 30B in PP/organoclay nanocomposite is increased to 6.15° indicating that PP is not able to improve the intercalating of Cloisite 30B organoclays.

Transmission electron microscopy (TEM)

To determine the dispersion and localization of Cloisite 30B in PBT/PP blend with and without PP-*g*-MA, transmission electron microscopy was performed. Figure 2a, b indicate the TEM photographs of BP30B5 and BP30B5C5 nanocomposites. The localization of Cloisite 30B around the domain boundaries is apparent in both Fig. 2a, b. As it can be seen in Fig. 2a, the excess parts of organoclays are localized in PBT matrix while some parts of organoclays migrate to PP dispersed-droplets in Fig. 2b. Therefore, it seems that compatibilizer can transfer some parts of organoclays from PBT matrix to PP dispersed-phase. Although there is satisfactory dispersion of Cloisite 30B layers in PBT matrix, but those parts of nanoclays located in PP droplets show poor intercalation structure which confirms the XRD analysis. Probably, the interaction between maleic anhydride group of PP-*g*-MA and hydroxyl groups of Cloisite 30B plays an important role in localization of some parts of Cloisite 30B in PP droplets. Due to hydrophobic nature of PP and the lack of any functional groups to react with hydroxyl groups of Cloisite 30B, PP is not able to intercalate into the gallery of Cloisite 30B nanoclays. The present outcome is in good agreement with the results of Fig. 1b. Hence, Fig. 2b shows the vice versa effect of PP-*g*-MA in dispersion and localization of Cloisite 30B organoclays in PBT/PP blend in comparison with the investigations of Xue et al. [4].

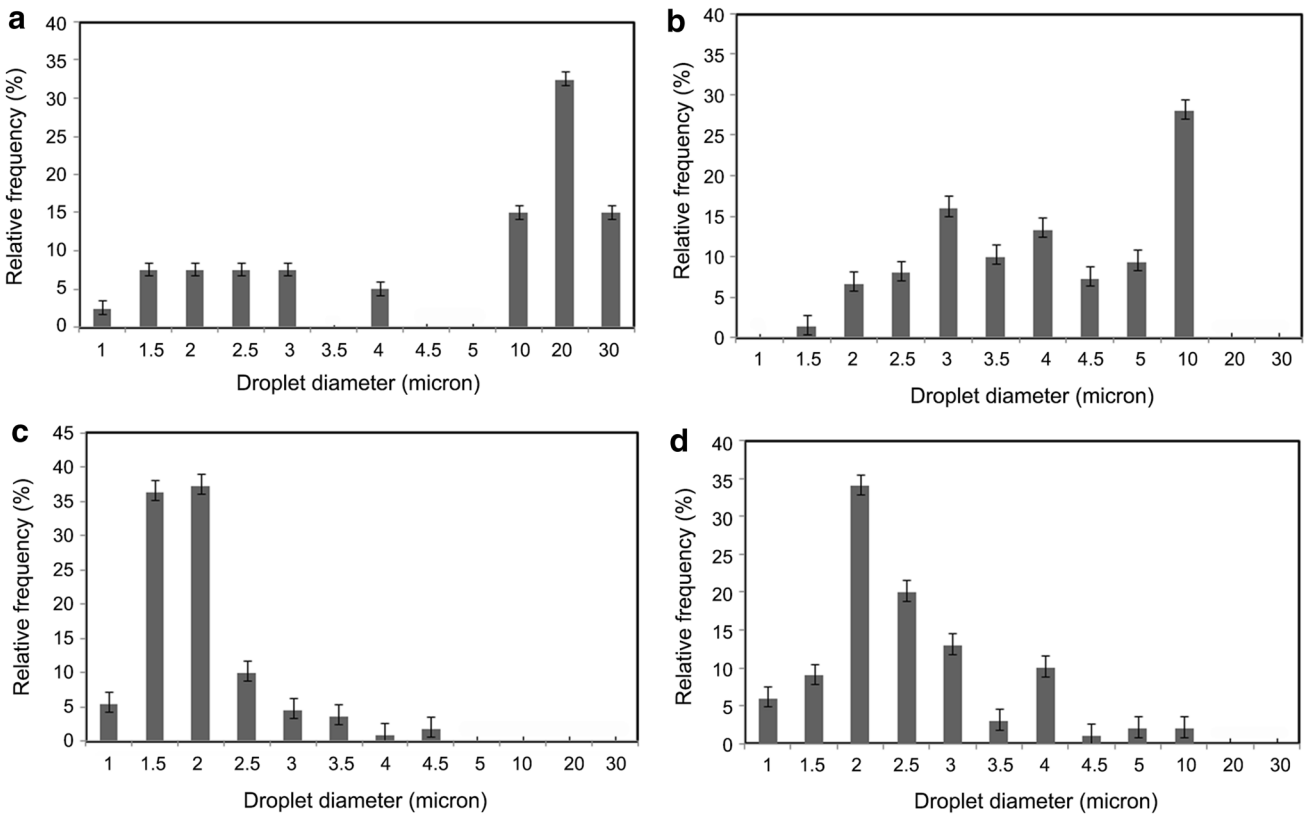

Fig. 4 Particle size distribution of **a** BP, **b** BPC5, **c** BP30B5 and **d** BP30B5C5

Morphological analysis by scanning electron microscopy (SEM)

Figure 3a–d illustrate the SEM photos of BP, BPC5, BP30B5 and BP30B5C5 samples. In Fig. 3a, PP domains easily detach from PBT matrix due to low interfacial adhesion in neat PBT/PP blend (BP sample). Nevertheless, the coarse detachment line of PP droplets in PBT/PP/organoclay nanocomposites (BP30B5 sample) represents satisfactory interfacial adhesion between the phases. In fact, the fractured surface in compatibilized PBT/PP blend (BPC5 sample) is not as coarse as BP30B5 and BP30B5C5 nanocomposites. So, it seems that Cloisite 30B organoclay is more effective than PP-*g*-MA in formation of interfacial interactions between PBT and PP. From Fig. 3b, c, adding PP-*g*-MA and Cloisite 30B to PBT/PP blend results in reduction of droplet size whereas the efficiency of Cloisite 30B organoclay in total seems to be higher than PP-*g*-MA. The role of Cloisite 30B in morphology development of PBT/PP blend was explained in our last work [21]. Comparing Fig. 3c, d indicates that the application of PP-*g*-MA along with Cloisite 30B (BP30B5C5 sample) results in a small increment of PP droplet size than BP30B5 nanocomposite. The presence of some parts of organoclays in PP phase (Fig. 2b) can cause the increment of dispersed-phase viscosity and elasticity which hinders droplets from breaking-up. To provide a quantitative investigation of the morphology of sample, the size of PP droplets was analyzed by image analysis software. Particle size distributions of BP, BPC5, BP30B5 and BP30B5C5 samples are illustrated in Fig. 4a–d. Obviously, neat PBT/PP blend shows larger droplet size with lower number. By adding PP-*g*-MA, Cloisite 30B and PP-*g*-MA/Cloisite 30B to PBT/PP blend, the number of droplets increases and their size decreases. If increases in droplet number and decreases in droplets diameter are considered as compatibilization efficiency indices, comparison of different systems would be classified in the following order according to lowering efficiency: Cloisite 30B > PP-*g*-MA/Cloisite 30B >> PP-*g*-MA.

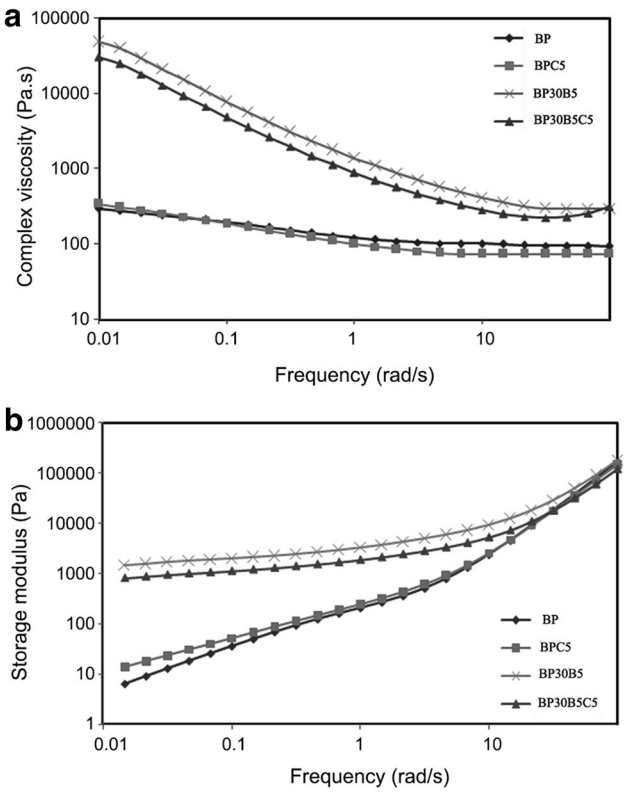

Fig. 5 **a** Complex viscosity and **b** storage modulus as a function of frequency for different samples

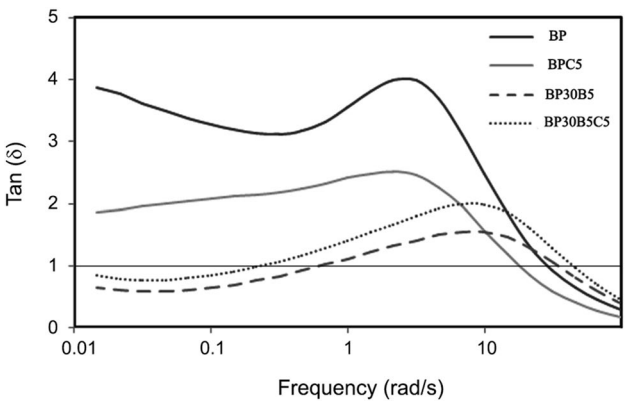

Fig. 6 Tan (δ) versus frequency for various specimens

Linear viscoelastic properties

Figure 5a, b represent the complex viscosity and storage modulus of various samples. The complex viscosity of PBT/PP compatibilized with PP-*g*-MA does not alter so much compared to neat PBT/PP blend. On the other hand, adding Cloisite 30B has great effect on growing of viscosity, especially at low frequency regions. This can be attributed to interactions formed between hydroxyl ethyl groups of Cloisite 30B and hydroxyl and carboxyl end groups of PBT. Using compatibilizer along with organoclay decreases the complex viscosity of nanocomposite compared to individual organoclay. Similar to complex viscosity, PP-*g*-MA does not affect the storage modulus of PBT/PP blend, so much. It might be relied on lower storage modulus of PP-*g*-MA than neat PP [22]. The storage modulus of blend enhances about 2 orders of magnitude by using 5 wt% of Cloisite 30B. Moreover, the non-terminal behavior is observed for samples containing organoclay (BP30B5 and BP30B5C5 samples). Accordingly, the viscoelastic behavior of nanocomposites changes from liquid-like to solid-like at low frequencies. By comparing the

storage modulus of BP30B5 and BP30B5C5 nanocomposites, one may notice that PP-*g*-MA together with Cloisite 30B decreases the storage modulus and elasticity of PBT/PP/organoclay nanocomposite. Moving to higher frequencies, the storage modulus of nanocomposites converges to the value of neat polymer blend which is due to alignment of organoclay layers.

To have a more comprehensive investigation regarding the contribution of compatibilizer and organoclay in the formation of interactions in PBT/PP blend, the curve of tan (δ) is plotted and shown in Fig. 6. Based on the results of tan (δ), the decrement of peak intensity for BP30B5 nanocomposite is more than other samples. Therefore, it can be concluded that individual Cloisite 30B is more efficient than PP-*g*-MA and PP-*g*-MA/Cloisite 30B system, in formation of elastic interactions. Using PP-*g*-MA/Cloisite 30B system is in the second place and PP-*g*-MA is in the third place in formation of elastic interactions. As we know it, when tan (δ) <1, the storage modulus will be higher than loss modulus and elastic behavior is dominant. According to Fig. 6, the tan (δ) values of BP30B5 and BP30B5C5 are lower than unity at low frequencies. This trend indicates greater elasticity of nanocomposites than BP and BPC5 samples because of better compatibility. The higher elasticity of nanocomposites in comparison with BP and BPC5 specimens may arise from clay–clay and/or PBT-clay interactions. These interactions can result in formation of three-dimensional physical networks which assist in coalescence suppression of dispersed-droplets. As it is clear, PBT/PP/Cloisite 30B nanocomposite (BP30B5) shows higher elasticity than PBT/PP/PP-*g*-MA/Cloisite 30B nanocomposite (BP30B5C5), at low frequency regions. The present subject indicates that PP-*g*-MA together with Cloisite 30B reduces the elasticity of PBT/PP/Cloisite 30B nanocomposite.

As discussed in previous sections, the interactions between hydroxyl ethyl groups of Cloisite 30B and hydroxyl and carboxyl end groups of PBT play an important role in formation of physical networks, improving viscosity, enhancement of elasticity and may cause coalescence suppression of droplets [23]. ATR-FTIR technique was used to probe these interactions. Figure 7a, b illustrate the FTIR spectra of neat PBT and PBT/Cloisite 30B (B30B5) nanocomposite, respectively. The band at

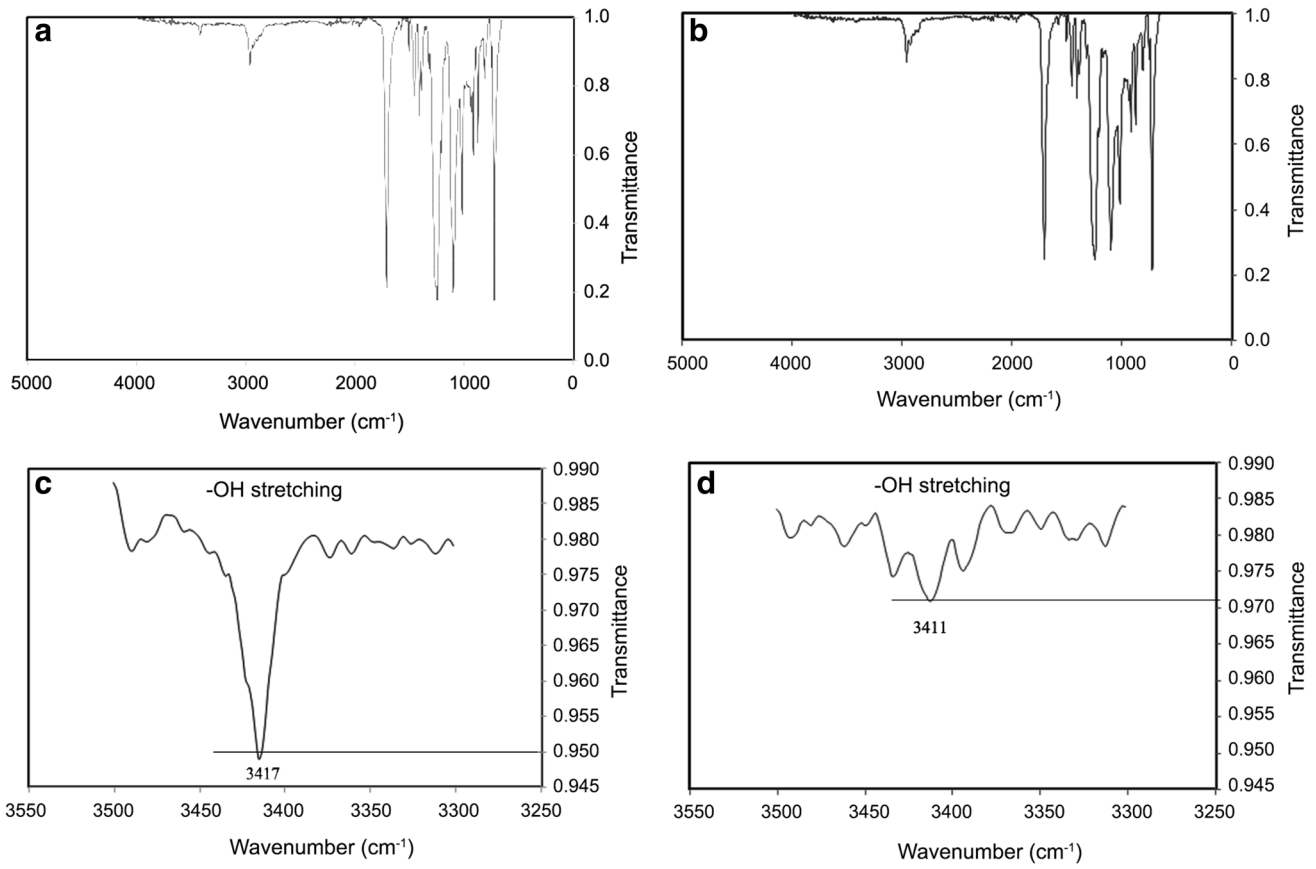

Fig. 7 FTIR spectra of **a** neat PBT in the wavenumber range of 650–4000 cm^{-1}, **b** PBT/Cloisite 30B nanocomposite in the range of 650–4000 cm^{-1}, **c** neat PBT in the range of 3250–3550 cm^{-1} and **d** PBT/Cloisite 30B nanocomposite in the range of 3250–3550 cm^{-1}

wavenumber of 3417 cm^{-1} is attributed to –OH stretching of PBT [24] which is magnified in Fig. 7c, d (wavenumber range of 3250–3550 cm^{-1}). It is observed that the –OH stretching band at 3417 cm^{-1} is affected in PBT/Cloisite 30B nanocomposite. The –OH stretching band of PBT/Cloisite 30B nanocomposite shifts to lower energy side by 6 cm^{-1} (3411 cm^{-1}). Moreover, the peak intensity of –OH stretching band decreases in PBT/Cloisite 30B nanocomposite compared to neat PBT. The present subject can be attributed to the interactions formed between hydroxyl end groups of PBT and hydroxyl groups of Cloisite 30B. As a result, the extra influence of Cloisite 30B relative to PP-*g*-MA on finer morphology and viscoelastic behavior of PBT/PP blend emanate from PBT-Cloisite 30B interactions.

Non-linear viscoelastic properties

As it was shown in linear viscoelastic section, adding 5 wt% of Cloisite 30B enhances the low frequency complex viscosity and storage modulus of PBT/PP blend. According to investigations of other researchers [22, 25], by increasing of clay concentration, the Newtonian plateau region in complex viscosity gradually disappears and storage modulus shows non-terminal behavior until percolation network is formed. At this point, nanocomposites represent a solid-like behavior with strong shear-thinning at low frequencies (like BP30B5 and BP30B5C5 samples in this research). The apparent yield stress is a result of percolation network and solid-like behavior. Higher apparent yield stress can be attributed to stronger clay–clay and/or polymer–clay interactions.

To further explore the microstructure of PBT/PP/organoclay and PBT/PP/PP-*g*-MA/organoclay nanocomposites, the start-up of shear flow experiment was carried out. Accordingly, BP30B5 and BP30B5C5 nanocomposites were imposed to start-up of flow at three different shear rates. The response of transient shear stress versus time is illustrated in Fig. 8a, b, for each nanocomposite. As it can be seen, both nanocomposites represent the stress overshoot whose magnitude increases by increasing of applied shear rate. The observed stress overshoot relies on the rupture of networks arising from orientation of organoclay platelets under shear flow. A comparison of Fig. 8a with b indicates that BP30B5 nanocomposite shows more intensified stress overshoot than BP30B5C5 sample in various applied shear rates. Based on the present subject, the strength of network interactions in PBT/PP blend filled by Cloisite 30B is higher than nanocomposite filled by PP-*g*-MA/Cloisite 30B system.

The stress relaxation behavior of BP30B5 and BP30B5C5 nanocomposites is illustrated in Fig. 9. In both nanocomposites, shear modulus tends to non-zero

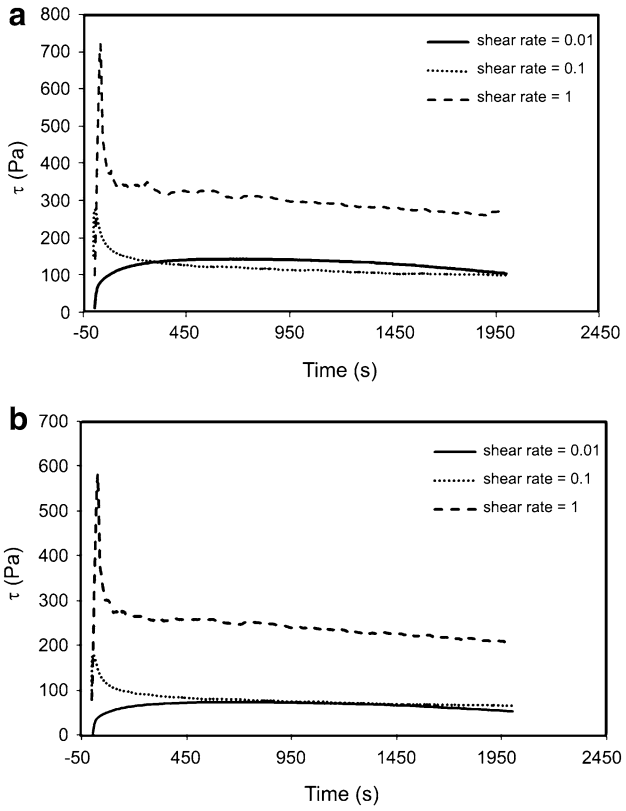

Fig. 8 Transient stress versus time in start-up of shear flow at different shear rates for **a** BP30B5 and **b** BP30B5C5 nanocomposites

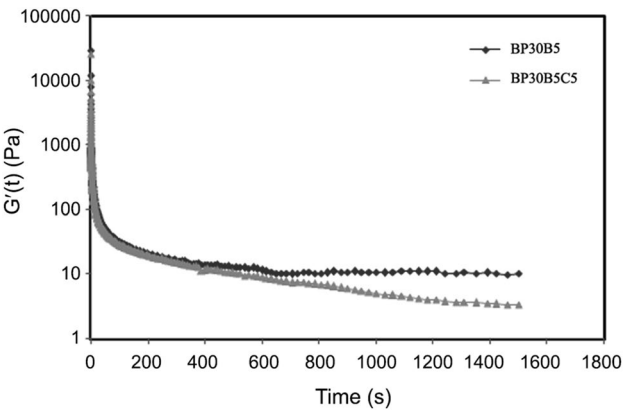

Fig. 9 Relaxation modulus versus time for BP30B5 and BP30B5C5 nanocomposites

values. This behavior is melting characteristic of solid-like structure and thixotropic behavior [26]. A similar behavior was reported by Nazockdast et al. [22] for PP/organoclay nanocomposites compatibilized by PP-*g*-MA. Obviously, the steady shear modulus of PBT/PP blend filled by Cloisite 30B is higher than sample containing Cloisite30B/PP-*g*-MA. From this result, it can be

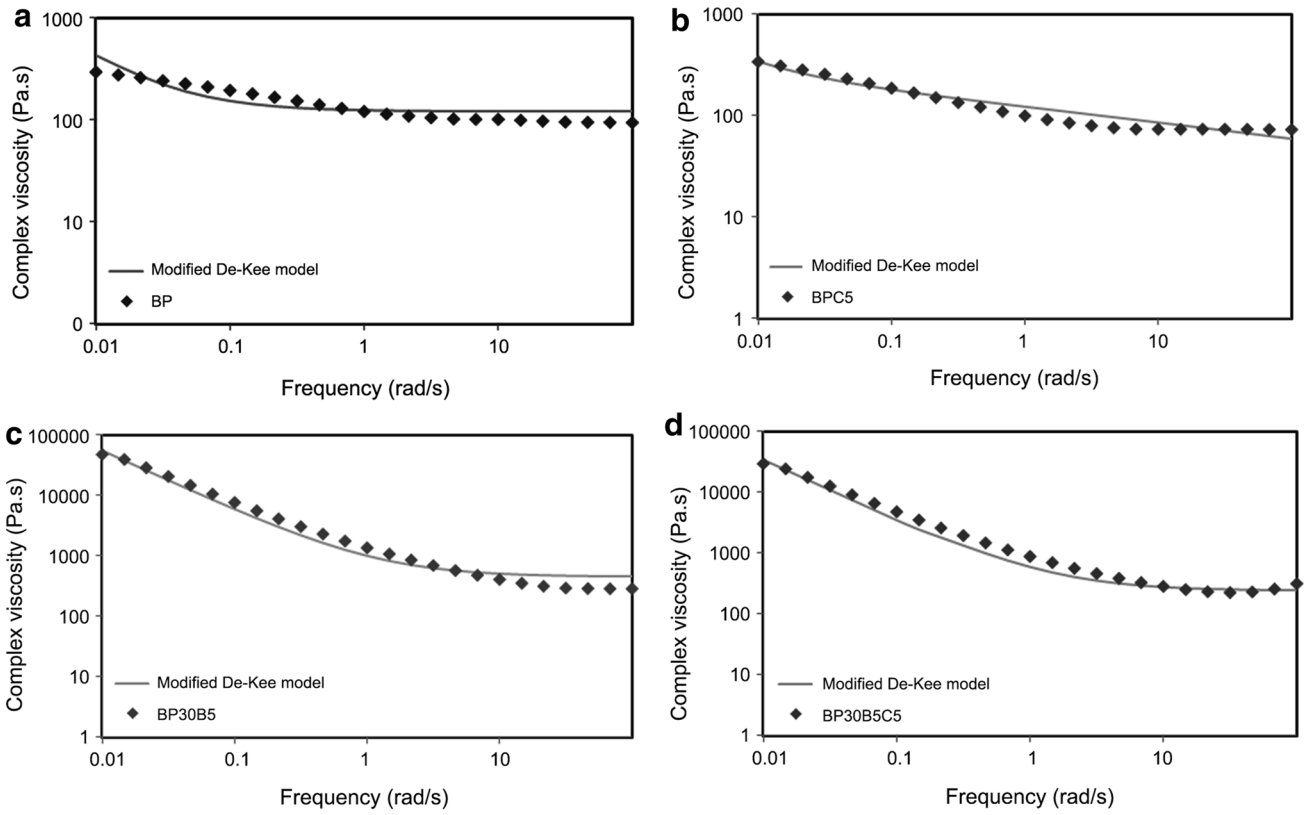

Fig. 10 The curve fitting of experimental viscosity data by modified De-Kee and Turcotte model for **a** BP, **b** BPC5, **c** BP30B5 and **d** BP30B5C5

Table 2 Modified De Kee-Turcotte model parameters for different samples

Sample	τ_0	η_1	t_1	α	R^2
BP	3.27	121.15	2.5×10^{-13}	−6.8	0.92
BPC5	1.06	200,782	7.41	0.02	0.97
BP30B5	551.8	454.2	9.2×10^{-17}	−3.3	0.99
BP30B5C5	352.27	240.02	5×10^{-6}	−4.1	0.99

concluded that the strength of physical network in PBT/PP/Cloisite 30B is higher than PBT/PP/PP-*g*-MA/Cloisite 30B nanocomposite.

Modeling

As declared in linear and non-linear viscoelastic properties sections, PBT/PP/Cloisite 30B (BP30B5) and PBT/PP/PP-*g*-MA/Cloisite 30B (BP30B5C5) nanocomposites show yield stress due to formation of three-dimensional physical networks. In 1980, De-Kee and Turcotte offered a three-parameter model [27, 28] (Eq. 1) for prediction of yield stress in systems containing solid networks.

$$\eta^* = \tau_0 \omega^{-1} + \eta_1 e^{-t_1 \omega} \quad (1)$$

In Eq. 1, η^* is complex viscosity, τ_0 includes a constant yield stress which is relied on the breakage of solid networks. The term of η_1 indicates zero viscosity in the absence of solid network and t_1 is characteristic time attributed to the velocity of the viscosity drop at higher frequencies [28]. Though, Carreau noticed that η_1 and t_1 are analytical model parameters and not as real material properties [29]. In 2010, Dorigato et al. [28] modified De-Kee and Turcotte model for nanocomposites containing silica nanoparticles (Eq. 2). They proposed a new parameter α which should improve the ability of model to follow the non-linear viscosity drop at high frequency regions

$$\eta^* = \tau_0 \omega^{-1} + \eta_1 e^{-t_1 \omega^{\alpha}} \quad (2)$$

Figure 10a–d show the curve fitting of experimental complex viscosity by modified De Kee-Turcotte model (Eq. 2), for different samples. According to correlation coefficient (R^2), there is satisfactory agreement between experimental data and modified De Kee-Turcotte model for BP30B5 and BP30B5C5 nanocomposites. As it is obvious, this model does not predict the complex viscosity of neat PBT/PP blend (BP sample), very well. There is some deviation between experimental data and the trend of De-Kee model in PBT/PP/PP-*g*-MA sample (BPC5), as well. Modified De Kee-Turcotte model parameters are represented in

Table 2. Clearly, BP and BPC5 samples do not show any strong yield stress (τ_0). According to approximation of modified De Kee-Turcotte model, BP30B5 and BP30B5C5 nanocomposites represent the yield stress (τ_0) of 551.8 and 352.27 Pa, respectively. It can be concluded that using PP-*g*-MA reduces the efficiency of Cloisite 30B organoclays in PBT/PP blend which results in lower yield stress.

Conclusion

The compatibilization effectiveness of PP-*g*-MA (conventional compatibilizer), Cloisite 30B (organoclay with hydrophilic modifier) and PP-*g*-MA/Cloisite 30B system in PBT/PP blend was investigated, in this research. According to X-ray diffractometry, the intercalated structure is achieved for PBT/organoclay, PBT/PP/organoclay and PBT/PP/PP-*g*-MA/organoclay nanocomposites, while there is no affinity between PP and Cloisite 30B in PP/organoclay sample. Moreover, inclusion of PP-*g*-MA reduces the intercalation level of Cloisite 30B in PBT/PP blend. Based on morphological analysis, Cloisite 30B organoclays result in the reduction of PP droplet size more pronounced than PP-*g*-MA. The finer morphology of different systems in PBT/PP blend can be classified as: Cloisite 30B > PP-*g*-MA/Cloisite 30B >> PP-*g*-MA. From linear melt rheology, it can be concluded that solitary Cloisite 30B is more effective than PP-*g*-MA in formation of elastic interactions. In addition, using PP-*g*-MA along with Cloisite 30B decreases the elasticity of PBT/PP/organoclay nanocomposite, due to transferring some parts of organoclay from PBT matrix to PP phase. Non-linear viscoelastic properties together with the results of modified De Kee-Turcotte model reveal that PBT/PP/organoclay nanocomposite indicates higher stress overshoot and yield stress than PBT/PP/PP-*g*-MA/organoclay related to stronger physical networks of organoclays.

References

1. Ezzati P, Ghasemi I, Karrabi M, Aziz H (2008) Rheological behaviour of PP/EPDM blend: the effect of compatibilization. Iran Polym J 17:669–679
2. Wu D, Zhou C, Zhang MJ (2006) Effect of clay on immiscible morphology of poly(butylene terephthalate)/polyethylene blend nanocomposites. J Appl Polym Sci 102:3628–3633
3. Pang YX, Jia DM, Hu HJ, Hourston DJ, Song M (2000) Effect of compatibilizing agent on morphology, interface and mechanical behavior of polypropylene/poly(ethylene terephtalate) blends. Polymer 41:357–365
4. Xue ML, Li P (2009) Phase morphology and clay distribution of poly(trimethylene terephthalate)/polypropylene/montmorillonite nanocomposites. J Appl Polym Sci 113:3883–3890
5. Shieh YT, Liao TN, Chang FC (2001) Reactive compatibilization of PP/PBT blends by a mixture of PP-*g*-MA and epoxy resin. J Appl Polym Sci 79:2272–2285
6. Tsai CH, Chang FC (1996) Polymer blends of PBT and PP compatibilized by ethylene-*co*-glycidyl methacrylate copolymers. J Appl Polym Sci 61:321–332
7. Bonda S, Mohanty S, Nayak SK (2014) Influence of compatibilizer on mechanical, morphological and rheological properties of PP/ABS blends. Iran Polym J 23:415–425
8. Djellali S, Haddaoui N, Sadoun T, Bergeret A, Grohens Y (2013) Structural, morphological and mechanical characteristics of polyethylene, poly(lactic acid) and poly(ethylene-*co*-glycidyl methacrylate) blends. Iran Polym J 22:245–257
9. Sun YJ, Hu GH, Lambla M, Kotlar HK (1996) In situ compatibilization of polypropylene/poly(butylene terephthalate) polymer blends by one-step reactive extrusion. Polymer 37:4119–4127
10. Papadopoulou CP, Kalfoglou NK (2000) Comparison of compatibilizer effectiveness for PET/PP blends: their mechanical, thermal and morphology characterization. Polymer 41:2543–2555
11. Hong JS, Namkung H, Ahn KH, Lee SJ, Kim C (2007) Interfacial tension reduction in PBT/PE/clay nanocomposite. Rheol Acta 46:469–478
12. Khatua BB, Lee DJ, Kim HY, Kim JK (2004) Effect of organoclay platelets on morphology of nylon-6 and poly(ethylene-*ran*-propylene) rubber blends. Macromolecules 37:2454–2459
13. Hong JS, Namkung H, Ahn KH, Lee SJ, Kim C (2006) The role of organically modified layered silicate in the breakup and coalescence of droplets in PBT/PE blends. Polymer 47:3967–3975
14. Minaei-Zaim M, Ghasemi I, Karrabi M, Aziz H (2012) Effect of injection molding parameters on properties of cross-linked low-density polyethylene/ethylene vinyl acetate/organoclay nanocomposite foams. Iran Polym J 21:537–546
15. Si M, Araki T, Ade H, Kilcoyne ALD, Fisher R, Sokolov JC, Rafailovich M (2006) Compatibilizing bulk polymer blends by using organoclays. Macromolecules 39:4793–4801
16. Calcagno CIW, Mariani CM, Teixeira SR, Mauler RS (2009) Morphology and crystallization behavior of the PP/PET nanocomposites. J Appl Polym Sci 111:29–36
17. Jafari SH, Asadinezhad A, Kalati Vahid A, Khonakdar HA, Wagenknecht U, Heinrich G (2012) Polypropylene/poly(trimethylene terephthalate) blend nanocomposite: a thermal properties study. Polym Plast Technol 51:682–688
18. Hajibaba A, Naderi G, Esmizadeh E, Ghoreishy MHR (2014) Morphology and dynamic-mechanical properties of PVC/NBR blends reinforced with two types of nanoparticles. J Compos Mater 48:131–141
19. Jafari SH, Kalati Vahid A, Khonakdar HA, Asadinezhad A, Wagenknecht U, Jehnichen D (2012) Crystallization and melting behavior of nanoclay-containing polypropylene/poly(trimethylene terephthalate) blends. Express Polym Lett 6:148–158
20. Haji Abdolrasouli M, Nazockdast H, Mir Mohamad Sadeghi G, Kaschta J (2015) Morphology development, melt linear viscoelastic properties and crystallinity of polylactide/polyethylene/organoclay blend nanocomposites. J Appl Polym Sci 132. doi:10.1002/app.41300
21. Hajibaba A, Masoomi M, Nazockdast H (2016) The role of hydrophilic organoclay in morphology development of poly(butylene terephthalate)/polypropylene blends. High Perform Polym 28:85–95
22. Nazockdast E, Nazockdast H, Goharpey F (2008) Linear and nonlinear melt-state viscoelastic properties of polypropylene/organoclay nanocomposites. Polym Eng Sci 48:1240–1249
23. Fenouillot F, Cassagnau P, Majeste JC (2009) Uneven distribution of nanoparticles in immiscible fluids: morphology development in polymer blends. Polymer 50:1333–1350
24. Katti DR, Katti KS, Raviprasad M, Gu C (2012) Role of polymer interactions with clays and modifiers on nanomechanical

properties and crystallinity in polymer clay nanocomposites. J Nanomater 2012:1–15. doi:10.1155/2012/341056
25. Chafidz A, Al-haj Ali M, Elleithy RJ (2011) Morphological, thermal, rheological, and mechanical properties of polypropylene-nanoclay composites prepared from masterbatch in a twin screw extruder. J Mater Sci 46:6075–6086
26. Doremus P, Piau JM (1991) Yield stress fluid. Structural model and transient shear flow behavior. J Non Newton Fluid Mech 39:335–352
27. De Kee D, Turcotte G (1980) Viscosity of biomaterials. Chem Eng Commun 6:273–282
28. Dorigato A, Pegoretti A, Penati A (2010) Linear low-density polyethylene/silica micro- and nanocomposites: dynamic rheological measurements and modeling. Express Polym Lett 4:115–129
29. Carreau PJ, De Kee D, Chhabra RP (1997) Rheology of polymeric systems. Hanser, Munich